COHERENT LIGHT PROPAGATION THROUGH A TURBULENT ATMOSPHERE: MEASUREMENTS OF THE OPTICAL FILTER FUNCTION

Peter M. Livingston, et al

Ballistic Research Laboratories
Aberdeen Proving Ground, Maryland

October 1969

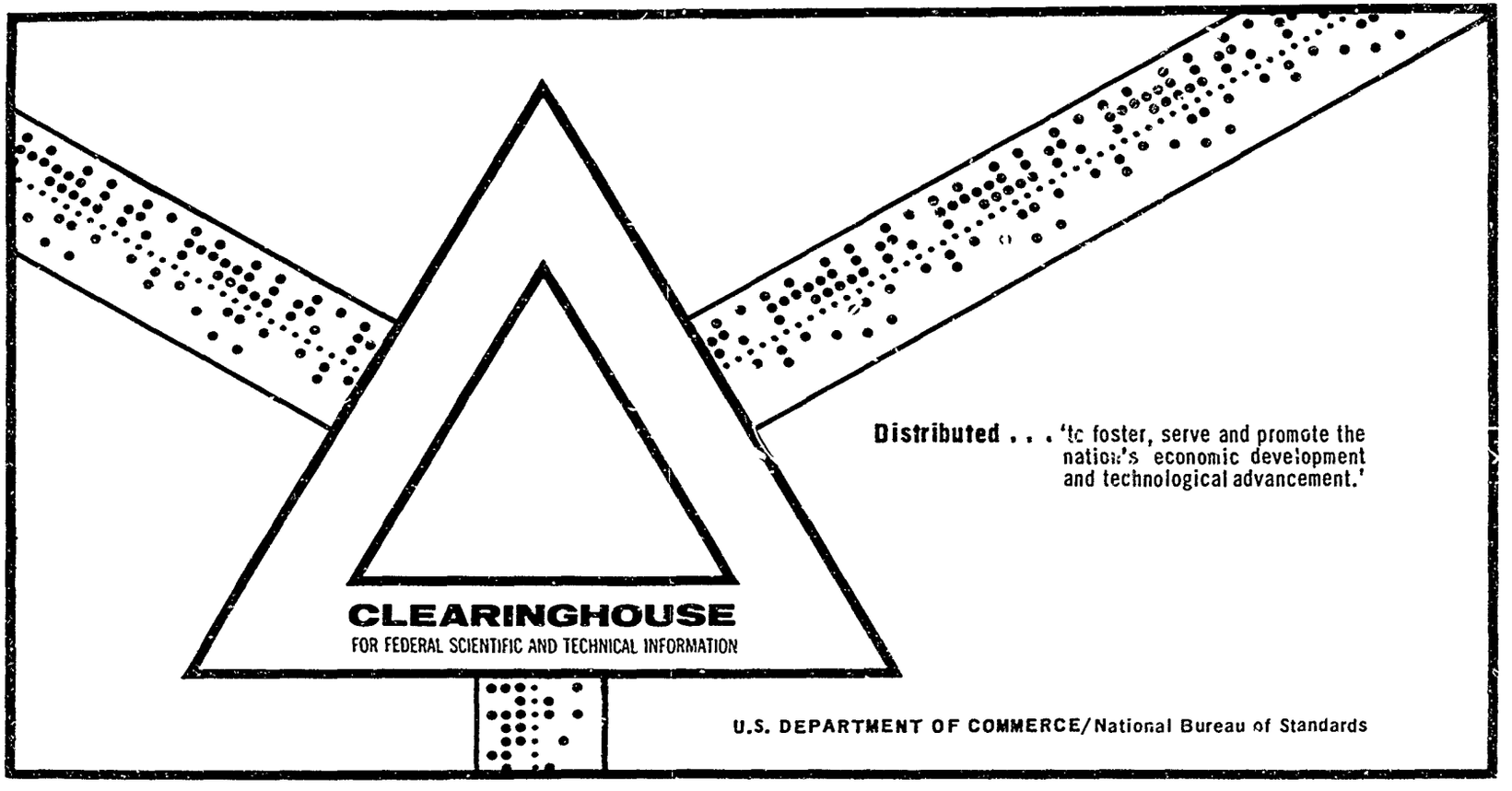

BRL MR 2018

BRL

AD

MEMORANDUM REPORT NO. 2018

COHERENT LIGHT PROPAGATION THROUGH A TURBULENT ATMOSPHERE: MEASUREMENTS OF THE OPTICAL FILTER FUNCTION

by

Peter M. Livingston
Paul H. Deitz
Ernest C. Alcaraz

October 1969

U.S. ARMY ABERDEEN RESEARCH AND DEVELOPMENT CENTER
BALLISTIC RESEARCH LABORATORIES
ABERDEEN PROVING GROUND, MARYLAND

B A L L I S T I C R E S E A R C H L A B O R A T O R I E S

MEMORANDUM REPORT NO. 2018

OCTOBER 1969

COHERENT LIGHT PROPAGATION THROUGH A TURBULENT ATMOSPHERE: MEASUREMENTS OF THE OPTICAL FILTER FUNCTION

Peter M. Livingston

Consultant to Signature and Propagation Laboratory

Paul H. Deitz
Ernest C. Alcaraz

Signature and Propagation Laboratory

RDTE Project No. 1T061102A31C

A B E R D E E N P R O V I N G G R O U N D, M A R Y L A N D

B A L L I S T I C R E S E A R C H L A B O R A T O R I E S

MEMORANDUM REPORT NO. 2018

PMLivingston/PHDeitz/ECAlcaraz/emj
Aberdeen Proving Ground, Md.
October 1969

COHERENT LIGHT PROPAGATION THROUGH A TURBULENT ATMOSPHERE: MEASUREMENTS OF THE OPTICAL FILTER FUNCTION

ABSTRACT

Two He-Ne lasers operating at 6328 Å have been utilized to make simultaneous measurements of the effects of scintillation over homogeneous optical paths of 650 and 1300 m to study the transfer of coherent radiation through a turbulent medium. At the path terminus, multiple sampling of each laser beam was effected using a photo-optical technique which records a 61-cm cross section of an optical beam. Concurrent with the optical data, wind-speed and direction recordings were made at multiple points along the optical path in order to estimate the homogeneity of meteorological conditions. Near the path terminus, measurements of wind shear and temperature lapse were taken. In addition, high-speed thermometry techniques were utilized to compute one-dimensional temperature spectra as well as the thermal structure coefficient C_T. Data were gathered during temperature-lapse, neutral, and inversion conditions. Log-irradiance scans derived from the optical data were used to compute log-irradiance power spectra, variance, and other statistical quantities. Using these optical and meteorological data, optical filter functions were then calculated for spatial frequencies above 87 c/m and are used to compare with current theories. The saturation of the log-irradiance data is again observed, and the isotropy of the irradiance fluctuations is examined.

TABLE OF CONTENTS

LIST OF ILLUSTRATIONS

INTRODUCTION

Light propagation through the lower atmosphere has received considerable attention in the past decade, both theoretically and experimentally. A recent review article by Strohbehn[1]* lists 59 references on the subject. Therefore, a detailed historical summary of the subject is omitted, but selections from current theoretical developments directly relevant to this paper are included.

It is well known that a light wave propagating through a region of turbulent atmosphere suffers phase and amplitude distortions as it progresses. If, instead of an infinite plane wave, a narrow beam is propagated through the medium, the center of energy of the beam can be observed to wander and the beam diameter to vary in time. The beam is being steered by passing through a set of spatially and temporally random refractive-index gradients. If the diameter of the beam is increased, marked irradiance variations (scintillations) become evident at sufficient ranges from the transmitter, while the beam steering effects are gradually reduced. For certain path-turbulence conditions, spectacular optical effects can occur, yielding large, irregular beam patterns. Finally, as the transmitted beam assumes a spherical wave front, the scintillation becomes independent of the transmitter and a function only of the spectral character of the atmospheric turbulence.

**References are listed on page 42.*

The three classes of optical effects--beam wander, diameter variation, and scintillation--are related directly to the low, medium, and high wave number regions, respectively, of the turbulence spectrum. The relative magnitudes of these three classes of optical effects are closely related to the transmitter-range parameters as well as to the variant character of the turbulence.

THEORETICAL BACKGROUND

Current light fluctuation theories may be classed according to whether single or multiple scattering is considered and whether the initial unperturbed wave is either an infinite plane (or spherical) wave or that of a finite beam. Of the single-scattering theories, the one formulated by Tatarski[2] is perhaps the most widely quoted. Tatarski considers a plane or spherical wave impinging on a slab of turbulent atmosphere whose statistics are known. For many systems applications, an actual source might be better described as a diffraction-limited beam with a gaussian transverse irradiance profile. Theories put forth by Ishimaru,[3] Carlson,[4] and Tatarski and Kon[5] describe such beam sources.

As might be expected, the introduction of an additional finite transmitter aperture changes the predicted statistics of the received light. Scintillation is produced by interference between scattered and unscattered portions of the beam. If, for a given range, the beam is sufficiently narrow so that the phase shifts between beam

elements are limited to much less than π radians, then irradiance variations may be largely eliminated. The predictions of phase and scintillation spectra, as well as phase and log-irradiance variances calculated by plane-wave single-scattering theory (PST) and beam-wave single-scattering theory (BST), are subject to experimental test as will be described below.

If the standard error of the measured log-irradiance of scintillation is plotted against the theoretical prediction obtained from PST for given turbulence-range parameters, it has been shown by Gracheva and Gurvich[6] in the Soviet Union, and verified by Deitz and Wright[7] and others in this country, that the statistics "saturate." That is, the measured statistics become nearly independent of the turbulence-range parameters beyond a certain critical value of the latter. Explanation of this phenomenon has stirred interest in multiple-scattering calculations, the chief contributors being Tatarski[8,9,10] and deWolf.[11] The plane-wave multiple-scattering theories (PMST) cited above do give rise to saturation curves; the one most cited is due to deWolf. However, the complex nature of these formulations has limited to date their application to predictions of log-irradiance variance; the transverse phase power spectra, for example, are not given by current PMST.

It is important to note that if the variance predicted by BST is plotted against the results predicted by PST, a linear relationship is not revealed either. The general features of the saturation measurements seem to be described by the formulation of Carlson,[4] but with

rather significant departures predicted at long ranges. Current experimental work is not yet adequate to make distinctions at long ranges.

We shall confine our comparison of the several theories to examination of scintillation. Let $\Phi_n^{(3)}(\kappa)$ be the isotropic three-dimensional power spectrum of the atmospheric refractive-index fluctuations at the spatial wave number κ. Let k be the optical wave number, L the path length, $\theta(\kappa)$ the optical filter function of the atmosphere, χ the (random) log-amplitude of the light wave, $\alpha = \lambda/\pi r_o^2$ the inverse Fresnel distance of an aperture of radius r_o, and $F_\chi(\kappa,0)$ the two-dimensional power spectrum of the beam cross section referred to object space. These quantities are related by

$$F_\chi(\kappa,\theta) = \pi k^2 L\, \theta(\kappa)\, \Phi_n^{(3)}(\kappa) \qquad (1)$$

for all first-order scattering theories. Now it is also true that the variance $\langle\chi^2\rangle(\langle\chi\rangle = 0)$ is given as the integral of F_χ where

$$\langle\chi^2\rangle = 2\pi \int_0^\infty F(\kappa,0)\, \kappa\, d\kappa. \qquad (2)$$

The variance may also be obtained by more direct averaging as in the case of PMST.

The quantities $\langle\chi^2\rangle F_\chi(\kappa,\theta)$ and $\Phi_n^{(3)}(\kappa)$ are all accessible through measurement. Consequently, it is possible to obtain the optical filter function by means of Eq. (1) and to compare this result along with the measured $\langle\chi^2\rangle$ with those predicted by theory. The formulations are given below. The PST gives[12]

$$\theta(\kappa) = 1 - \frac{k}{\kappa^2 L} \sin\left[\frac{\kappa^2 L}{k}\right], \tag{3}$$

$$\langle \chi_T^2 \rangle = 0.307\, C_n^2\, k^{7/6}\, L^{11/6}, \tag{4}$$

whereas BST[3,4] predicts

$$\theta(\kappa) = \frac{1}{2}\left(\frac{\pi}{qb}\right)^{1/2} \operatorname{erf}\left[(qb)^{1/2}\right] - \operatorname{Re}\left[\frac{1}{2}\left(\frac{\pi}{qb_1}\right)^{1/2} \exp(-q/4b_1) \times \left\{\operatorname{erf}\left(\frac{-i(q)^{1/2}}{2(b_1)^{1/2}} + (qb_1)^{1/2}\right) - \operatorname{erf}\left(\frac{-i(q)^{1/2}}{2(b_1)^{1/2}}\right)\right\}\right], \tag{5}$$

where

$$q = \frac{\kappa^2 L}{k}, \quad b = \frac{\alpha L}{1 + \alpha^2 L}, \quad \text{and} \quad b_1 = \frac{\alpha L}{1 - i\alpha L}. \tag{6}$$

The variance in the BST is given by

$$\langle \chi^2 \rangle = \pi^2\, 0.033\, C_n^2\, \Gamma(-5/6)\, k^{7/6}\, L^{11/6} \left[\frac{\alpha L}{1 + \alpha^2 L^2}\right]^{5/6} \left[\frac{3}{8} - g(\alpha L)\right], \tag{7}$$

where

$$g(\alpha L) = \operatorname{Re}\left[\frac{6}{11}\left(\frac{1 + i\alpha L}{i\alpha L}\right)^{5/6} {}_2F_1\left(\frac{-5}{6} ; 1 ; \frac{17}{6} ; i\alpha L\right)\right]. \tag{8}$$

Finally, PMST predicts a variance of

$$\langle \chi^2 \rangle = \frac{1}{4} \ln\left[2 - \exp(-4 \langle \chi_T^2 \rangle)\right]. \tag{9}$$

Plots of the optical filter functions described by Eqs. (3) and (5) are shown in comparison with experimentally derived curves at 650- and 1300-m ranges in Figs. 1 and 2. The log-irradiance statistics

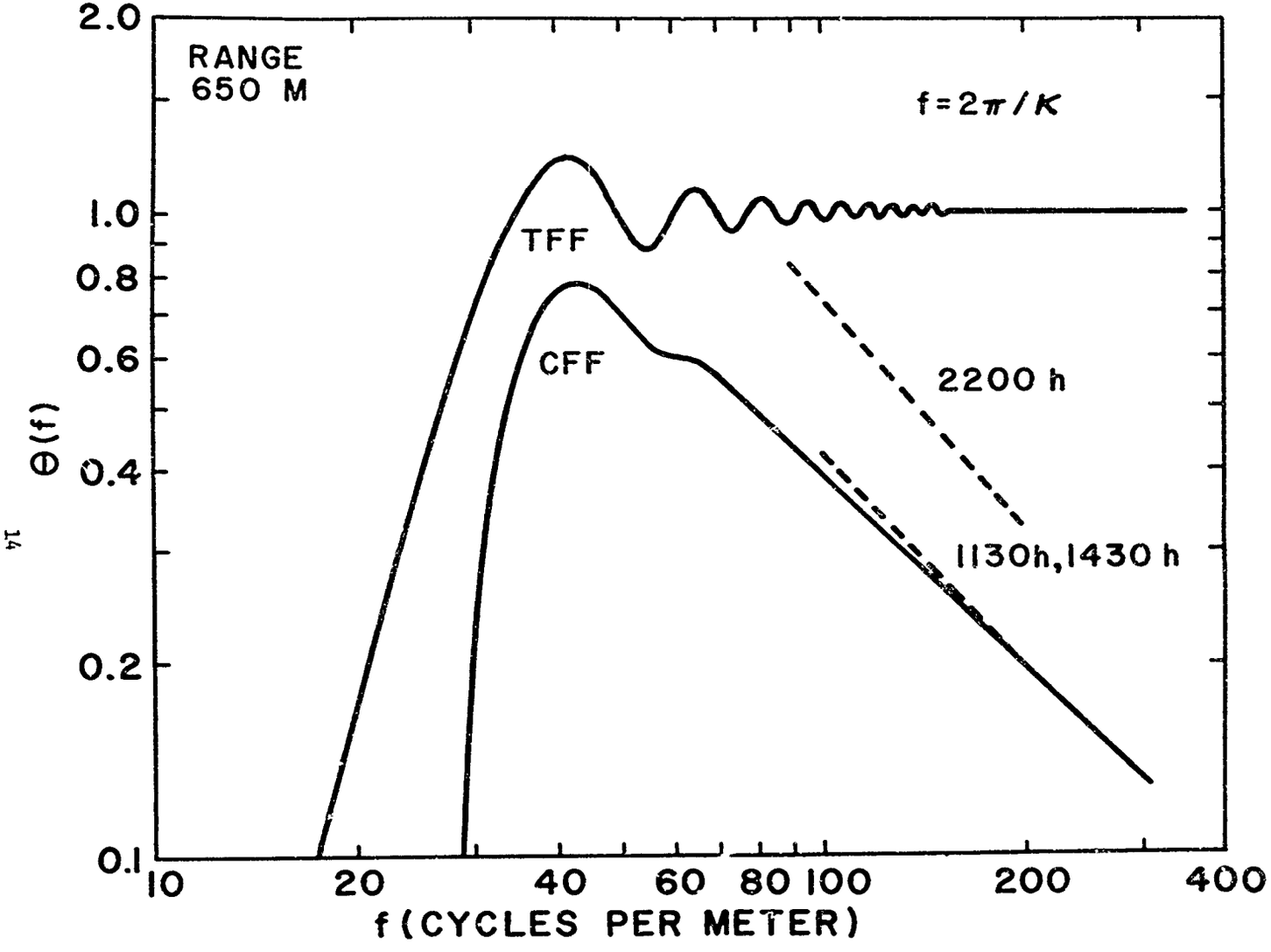

Figure 1. The Optical Filter Function, $\theta(f)$, as a Function of Spatial Frequency. The predictions of Tatarski (TFF) and Carlson and Ishimaru (CFF) are shown in solid lines, and experimental results for several times are shown in broken lines for a range of 650 m.

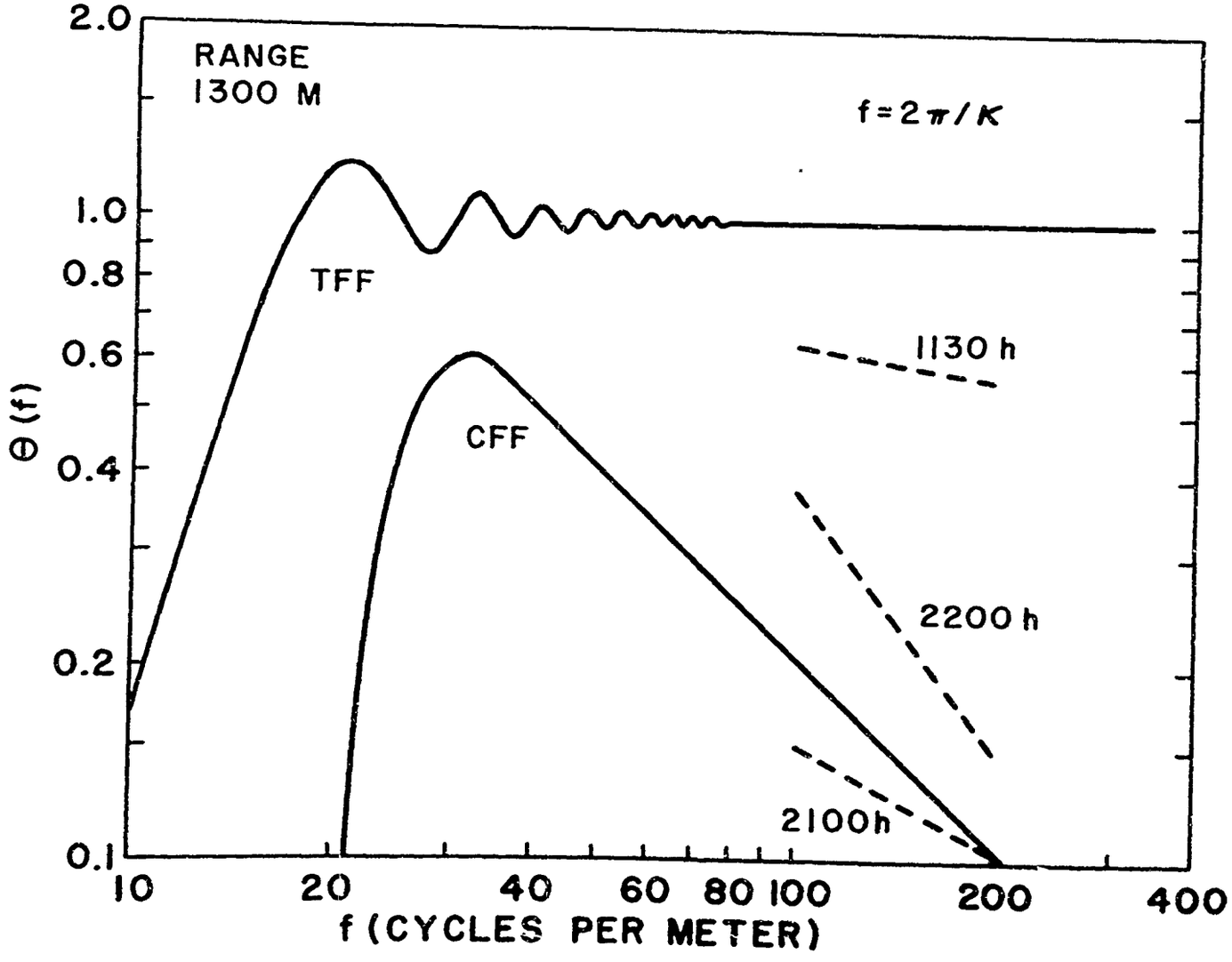

Figure 2. The Optical Filter Function, $\theta(f)$, as a Function of Spatial Frequency. The predictions of Tatarski (TFF) and Carlson and Ishimaru (CFF) are shown in solid lines, and experimental results for several times are shown in broken lines for a range of 1300 m.

are presented in Fig. 3. In the latter, twice the square root of $\langle \chi_T^2 \rangle$ is plotted along the abscissa, and the other theoretical results [Eqs. (4), (7), and (9)] are shown as appropriately identified curves. The spread in the data and the uncertainty in the measurements are shown by the error curves.

THE EXPERIMENT

Full documentation of an optical propagation experiment suggests detailed measurement of high-frequency temperature and velocity statistics at multiple points along the optical path. Such an approach is, of course, limited by practical considerations. The ideal optical experiment is conducted over a uniform terrain above which statistically homogeneous turbulence is maintained. For such conditions, detailed measurement of the microtemperature structure and fluctuation power spectra need be made at only one point. A useful compromise under practical conditions is to make the detailed measurements at one or more points near the beam and to record the gross meteorological conditions contained in wind-speed and direction measurements at a number of points and altitudes along the path. The gross measurements thus serve to test for homogeneity of conditions.

The BRL Optical Propagation Range, at which the experiments were conducted, is a leveled grass field. Local obstacles were removed to maintain homogeneous turbulence for specific wind directions.[13] A 650-m section of the optical range was instrumented at 152-m intervals

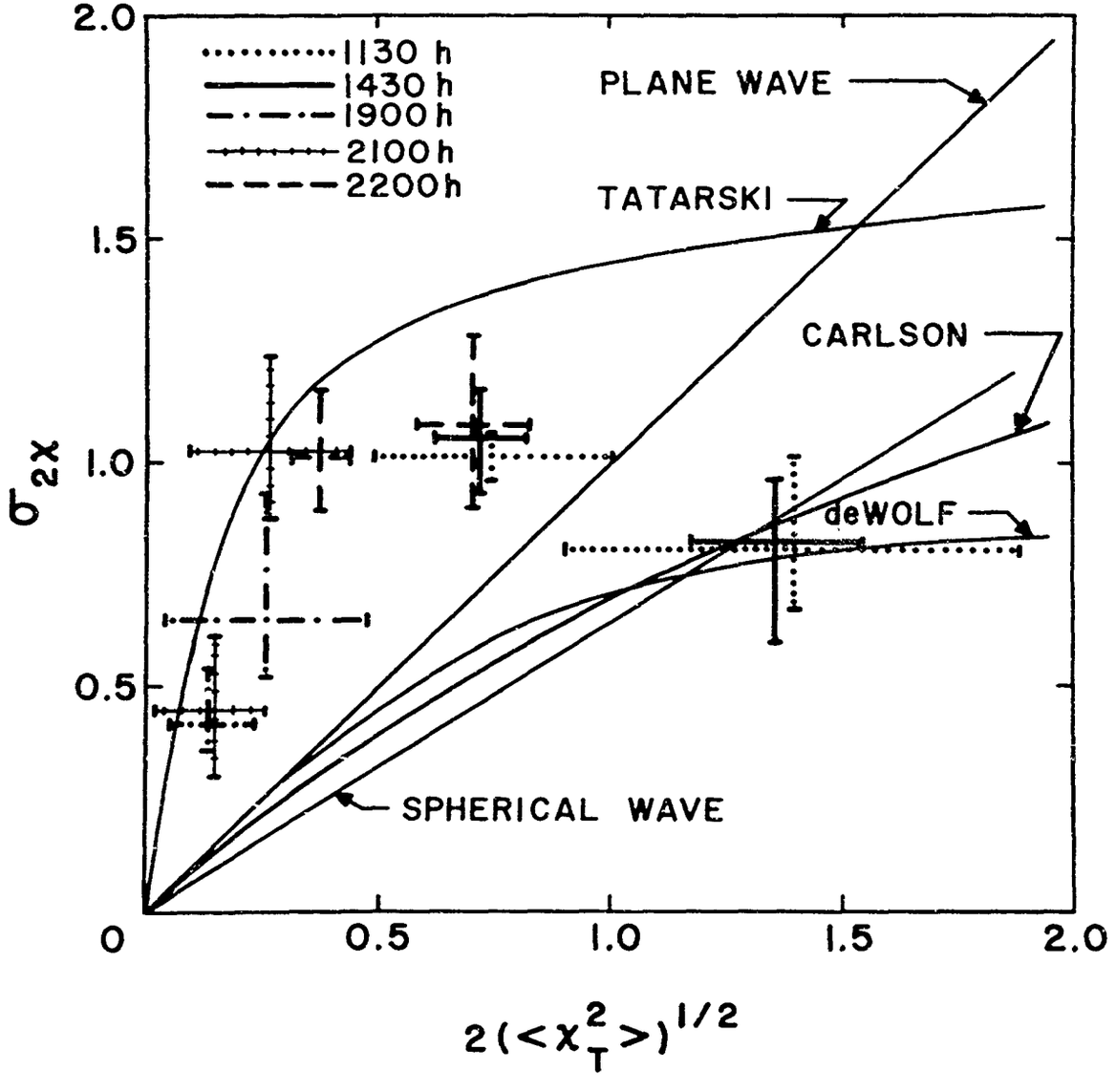

Figure 3. Standard Errors of Log-Irradiance as a Function of the Plane Wave Tatarski Prediction

with wind-speed and direction sensors and low-frequency thermometers. At each of five locations, a set of sensors was mounted on poles adjacent to the optical path at heights of 2.5, 5.2, and 9.4 m. The outputs of these sensors were selectively scanned and recorded by an analog-to-digital conversion system. An additional set of five wind-direction indicators having capability of real-time readout was installed adjacent to the optical path so that optimum times could be chosen for data acquisition.

As evident by Eqs. (4) and (7), the refractive-index structure constant C_n is the measure of turbulence power entering the expression of scintillation variance. Provided an "inertial subrange" of turbulence exists described by a Kolmogoroff velocity spectrum and that temperature inhomogeneities can be treated as conservative passive additives,[14] then the mean-square fluctuation of temperature is given by

$$\langle [T(\underline{r}_1) - T(\underline{r}_2)]^2 \rangle \equiv D_T(|\underline{r}_1 - \underline{r}_2|) = C_T^2 |\underline{r}_1 - \underline{r}_2|^{2/3}. \qquad (10)$$

Electrical measurement of the left side of Eq. (10) by means of cold-wire resistance thermometers at two fixed points, r_1 and r_2,[7] and suitable difference-squaring and averaging leads to the universal thermal structure constant C_T. For slow density variations characteristic of turbulence, the atmosphere is approximately incompressible. Therefore, the refractive-index structure constant C_n is given by a simplified Barrel-Sears formula[15] where

$$C_n = \frac{79 \times 10^{-6}}{T^2} p\, C_T, \tag{11}$$

where p is the atmospheric pressure in millibars and T is the absolute temperature.

The temperature structure constant may also be inferred by measurement of the vertical wind velocity and temperature profiles by the computation of the approximate Richardson number where

$$Ri = \frac{g(\overline{T}_1 - \overline{T}_2)\,(z_1 z_2)^{\frac{1}{2}}}{T_{amb}(\overline{V}_1 - \overline{V}_2)^2} \log(z_1/z_2);\ g = 980\ \text{cm/sec}^2. \tag{12}$$

An average Ri for pairs of points measured is readily computed. Theory and measurements by Tsvang[16] indicate that

$$C_T = f(Ri). \tag{13}$$

Values of C_T were derived through use of Tsvang's published curve. Conversions were then made of C_T to C_n.

Measurements of the structure constant by both the differential-probe and the Richardson-number methods are given in Table I. Probe separations of 10 and 36 cm were used in the differential technique. The vertical temperature and average wind velocity gradients were sampled at five logarithmically spaced altitudes to a maximum height of 8 m. A second, and independent, measure of C_T, as well as the spectrum of microtemperature fluctuations, was made[17] utilizing a modified single cold-wire probe. The index of refraction spectra, derived from the microtemperature spectra by applying the Barrel-Sears conversion factor, are shown in Figs. 4A and 4B.

TABLE I

METEOROLOGICAL DATA

Time	Normal Wind Speed (cm/sec)	R_i	C_N ($m^{-1/3}$)			
			Thornthwaite	Flow		Univ. of Mich.
				10 cm	36 cm	
1125-1135	232	-0.159	1.91×10^{-7}	1.5×10^{-7}	1.0×10^{-7}	1.31×10^{-7}
1425-1435	216	-0.217	1.61×10^{-7}		1.4×10^{-7}	1.21×10^{-7}
1855-1905	92	0.146	1.54×10^{-7}	2.1×10^{-7}	4.6×10^{-8}	1.21×10^{-8}
2105-2115	13	0.162	1.75×10^{-7}	2.7×10^{-8}	2.9×10^{-8}	1.06×10^{-7}
2155-2205	40	0.482	8.86×10^{-8}	6.0×10^{-8}	6.5×10^{-8}	8.25×10^{-8}

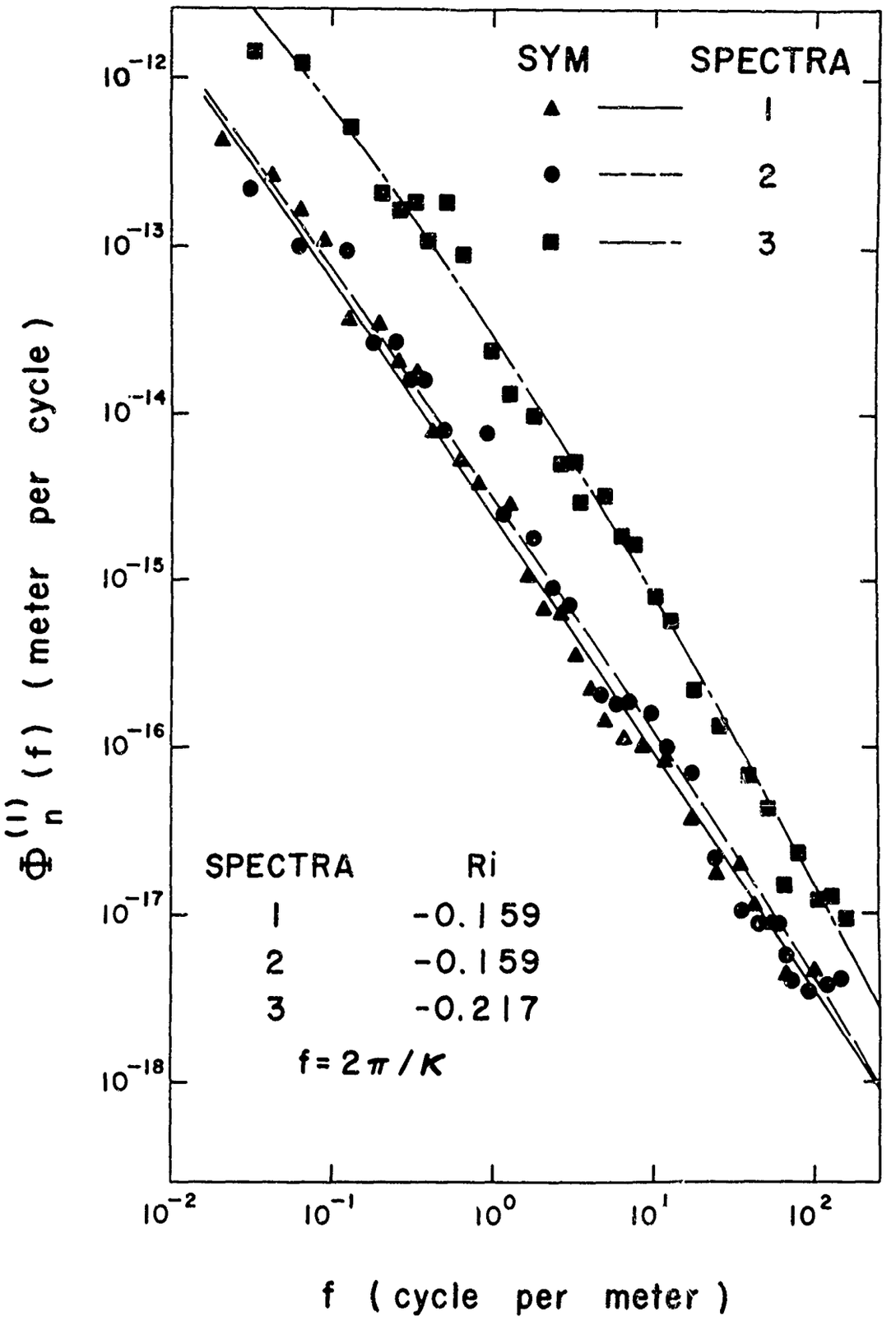

Figure 4A. Index of refraction spectra and the corresponding Ri estimate are given above for each curve. Spectra were measured by Portman and co-workers. Associated times are 1130h (1 and 2) and 1430h (3).

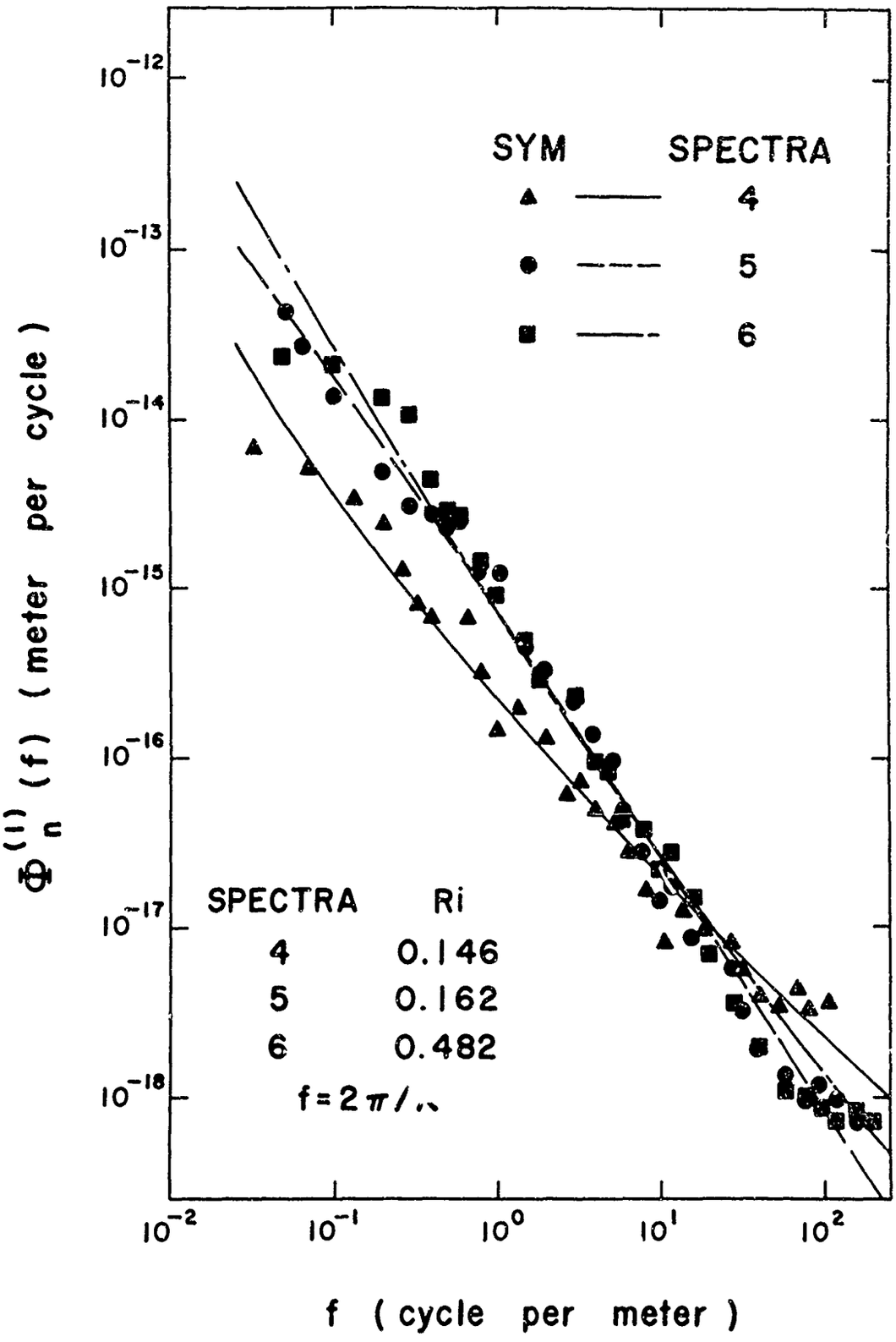

Figure 4B. Index of refraction spectra and the corresponding Ri estimate are given above for each curve. Spectra were measured by Portman and co-workers. Associated times are 1900h (4), 2100h (5), and 2200h (6).

Micrometeorological and optical data taken on 14 June 1968 can be characterized by the vertical temperature gradient. The first two data runs (1130 and 1430 h) took place during temperature lapse conditions, the third (1900 h) during approximately neutral, and the final two (2130 and 2200 h) occurred during inversion conditions. The day was clear with less than five percent cloud cover, thus minimizing variant solar absorption at the ground. The statistics for the meteorological tables were computed from ten-minute data runs. The indicated times correspond to the middle of the run and the time at which the optical data were taken.

For the optical measurements, two He-Ne lasers operating at 6328 Å were utilized. Each laser output was collimated through a telescope employing a spatial filter to remove variations in the wave front. Both beams were then adjusted to a divergence of 1.9 mrad, since this parameter has been found to be a factor in the resulting irradiance fluctuations.[7,18] One of the lasers was located at the south end of the propagation range and directed north over the 650-m path to an optical receiver system. The second laser was positioned adjacent to the receiver and directed toward the south end of the range. An optical flat, located next to the first laser, redirected the beam northward to be recorded.

The optical receiver system, essentially a telescope with a 61-cm primary element, is arranged with the image plane conjugate to the entrance aperture. Placing photographic film at the image and using

an appropriately short exposure time, a time-frozen recording can be made of the turbulence fluctuations in the laser beam. The calibrations and method of data extraction by this technique have been earlier documented.[7,18] This method has certain advantages over temporal sensing techniques. Microdensitometer scans of these photographs allow measurements to be made directly in the spatial domain, thus avoiding the inherent approximations of converting temporal fluctuations by use of the wind component normal to the optical path. Further, no assumption need be made about the degree to which the fluctuations are "frozen in."[19] In addition, scans may be made through the image in any direction, including the vertical, making possible examination of the isotropy of the irradiance fluctuations.

Five sets of optical data were taken corresponding to the five times[20] indicated in the meteorological table. At each period, three successive photographs were made of the laser beam cross section at 1300 m using an exposure time of 2 msec. Immediately following, three photographs, taken at the same exposure time, were made at the 650-m range. Thus, the six photographs taken during each run were acquired over an interval of about 30 sec. A horizontal, vertical, and two diagonal scans were made of each photograph using a microdensitometer with an effective aperture (referred to object space) of 0.4 × 3 mm. Corrections for this aperture are contained in the composite measured transfer function made for this instrument.

DATA REDUCTION

Digitized data, obtained from the densitometer scans of the photographs, were processed according to the flow diagram given in Fig. 5. A step tablet with approximately thirteen steps, photographed with the optical data, established the characteristic curve of the film. Previous measurements of the optical system have indicated that through the spatial frequency range of interest the transfer function of the optics is effectively unity. Hence, the major transfer function for which to account was that of the densitometer. The measured function was fitted to a sinc^2 function where

$$T_3(\kappa) = \text{sinc}^2(0.00154\kappa/2) \tag{14}$$

where κ is the spatial wave number in inverse meters. The standard errors of the irradiance and the log-irradiance data were computed in Programs I and II as shown in Table II. Since for normally distributed data

$$\sigma_{2\chi}^2 = \ln(1 + \sigma_I^2); \quad \overline{I} = 1, \tag{15}$$

where σ_I^2 is the variance of the irradiance data, it follows that a measurement of $\sigma_{2\chi}$ directly along with σ_I is a measure of the log-normality of the statistics. The column in Table II marked "corrected scale ratio" gives the number of irradiance correlation intervals across the scanned portion of the mirror. The defining expression is

$$\text{Corrected Scale Ratio} = \frac{500\ \sigma_I^2}{2\int_0^\infty B_I(l)\ dl} \tag{16}$$

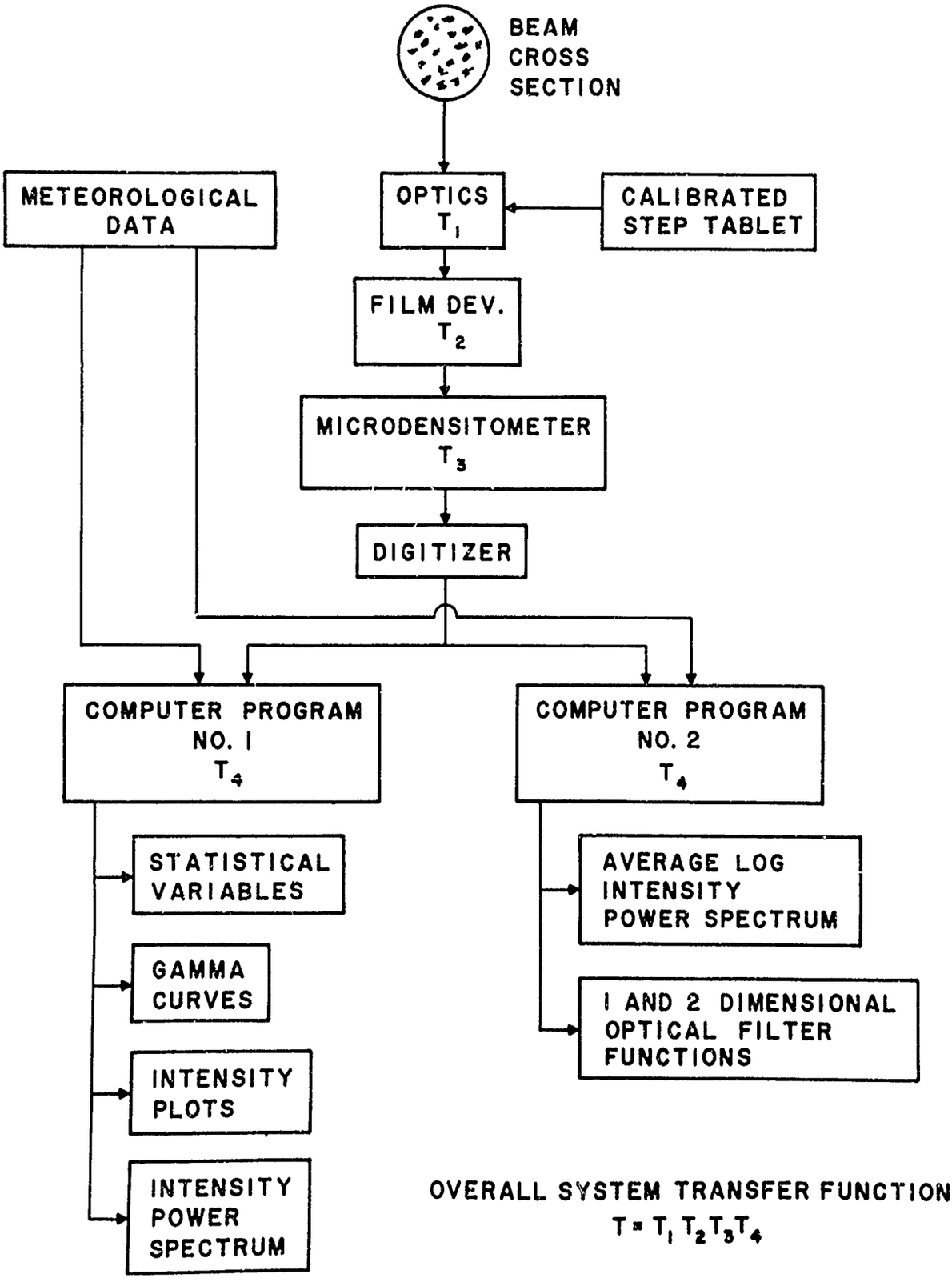

Figure 5. Data Reduction Flow Diagram

The individual subsystem transfer functions are represented by T_1 through T_4 and the overall system transfer function by T.

TABLE II

STATISTICAL AVERAGES

Time	Range	$\sigma_{2\chi}$	$\sigma^*_{2\chi}$	Corrected Scale Ratio
1130	650	1.036	1.018	25.29
	1300	0.676	0.811	30.35
1430	650	1.042	1.050	24.82
	1300	0.682	0.823	31.81
1900	650	0.498	0.444	10.87
	1300	0.634	0.656	19.80
2100	650	0.446	0.413	18.49
	1300	1.040	1.022	22.83
2200	650	1.023	1.027	24.01
	1300	0.936	1.084	23.57

$$\sigma^*_{2\chi} = [\ln(1 + \sigma_I^2 / \bar{I}^2)]^{\frac{1}{2}}$$

Here, $B_I(1)$ is the irradiance correlation function. Low-frequency disturbances due to the collimation problem were removed in Program I by a three-section variable mean and in Program II by a 20-point high-pass digital filter.[21] In addition to various displays of the statistics of the log-irradiance, the one-dimensional scan power spectra were calculated by the usual technique[22] after prefiltering the data. The set of one-dimensional scan spectra for each scan direction (horizontal, vertical, and two diagonal) and at each range time was then examined for anisotropy. Finally, the results for each scan direction were averaged at a given range time to produce 10 one-dimensional composite spectra from an original 120 scans.*

As an aid to further data analysis, the one-dimensional scan spectra described above were fitted to the form

$$P(f) = P(f_o)\ \exp[A\ln(f/f_o) + B\{\ln(f/f_o)\}^2], \qquad (17)$$

where f_o is an arbitrary reference frequency. Clearly, if $B = 0$, the power spectrum is a simple power law. Denoting by a superscript the dimension of the spectrum, the relation between the isotropic three-dimensional spectra and its associated one-dimensional spectra is given by

$$\Phi^{(3)}(\kappa) = \frac{-1}{2\pi\kappa}\ \frac{d}{d\kappa}\ \Phi^{(1)}(\kappa). \qquad (18)$$

A two-dimensional power spectrum is related to the one-dimensional quantity by

Through contractual arrangements with Photometrics, Inc., a separate program was undertaken for film scanning and power-spectrum analysis of the identical data. The results of these efforts are in direct agreement with those reported here.

$$\phi^{(2)}(\kappa) = \int_{-\infty}^{\infty} d\gamma\, \phi^{(3)}\left[(\gamma^2 + \kappa^2)^{\frac{1}{2}}\right]$$

$$= \frac{-1}{2\pi} \int_{-\infty}^{\infty} d\gamma\, \frac{1}{(\gamma^2 + \kappa^2)^{\frac{1}{2}}}\, \frac{d}{d(\gamma^2 + \kappa^2)^{\frac{1}{2}}}\, \phi^{(1)}\left[(\gamma^2 + \kappa^2)^{\frac{1}{2}}\right] \tag{19}$$

In Appendix A it is shown that with the curve fit, Eq. (17), the above equation may be expressed as

$$\phi^{(2)}(\kappa) = \frac{-\phi^{(1)}(\kappa)}{2\pi}\, \frac{d}{d\kappa}\, e^{a(\theta)} \sum_{k=0}^{\infty} \frac{1}{(4B)^k}\, \frac{\kappa^{2k}}{k!}\, \frac{d^{2k}}{d\kappa^{2k}}\, \beta(|A - 1 + 2\theta B|;\ 1/2), \tag{20}$$

where

$$\theta = \ln(\kappa/\kappa_o), \quad a(\theta) = A\theta + B\theta^2, \tag{21}$$

and $B(|A - 1 + 2\,\theta\, B|;\ 1/2)$ is the beta function. Equation (20) is best reduced further by numerical methods in terms of tabulated ψ functions. Another approach, and one used here, is an asymptotic, or saddle point, evaluation of the integral in Eq. (19).

The average one-dimensional scan spectra are converted to two-dimensional log-irradiance transverse power spectra by means of Eq. (20). Processing the one-dimensional temperature fluctuation spectra by means of Eqs. (17) and (18), the resultant isotropic temperature spectrum divided into the two-dimensional log-irradiance scan spectrum gives the optical filter function (OFF) as shown in Eq. (1). The OFF's for 650 m and 1300 m at particular range times are shown in Figs. 1 and 2.

RESULTS AND DISCUSSION

A. Apparent Atmospheric Anisotropy

In general, the one-dimensional log-irradiance scan spectra in horizontal and vertical directions showed marked differences as a function of frequency. A typical example is shown in Fig. 6. The ratio of horizontal to vertical power is plotted as a function of frequency for the 1400-h (lapse), 650- and 1300-m data. There is clearly a systematic decrease of the high-frequency power in the horizontal spectrum compared with the vertical spectrum. This result might be interpreted as a horizontal elongation, characteristic of the irradiance cells, or as being due to an exposure effect wherein the shortest wavelengths are transported an appreciable fraction of their length by the average normal wind component during the 2-msec exposure. An estimation of a wind transfer function for an ideal case is made in Appendix B. However, Fig. 7 shows horizontal and vertical spectra taken from a photograph of a pulsed ruby laser[7] with a 30-nsec pulse duration. The anisotropy of the previous figure is therefore a function of exposure time.

B. Average Scan Spectra

For a given range time, the four individual scan spectra taken from the three photographs were averaged together, thus reducing the statistical variation. Samples of these spectra and associated beam photographs are shown in Figs. 8, 9, 10, 11, 12, and 13. The first photograph-spectra pair gives typical results for lapse conditions

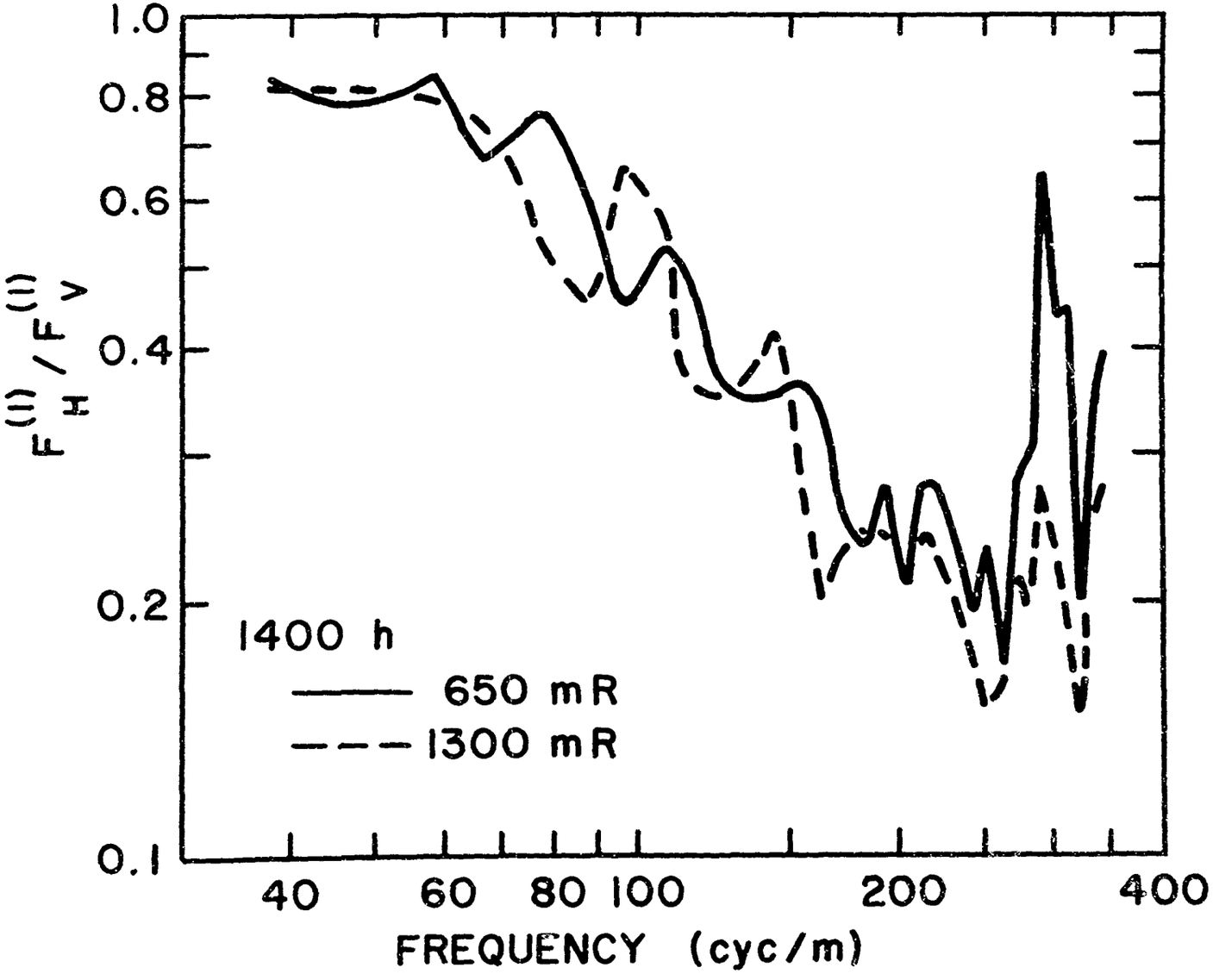

Figure 6. Ratio of Vertical to Horizontal Scan Power Spectra as a Function of Spatial Frequency

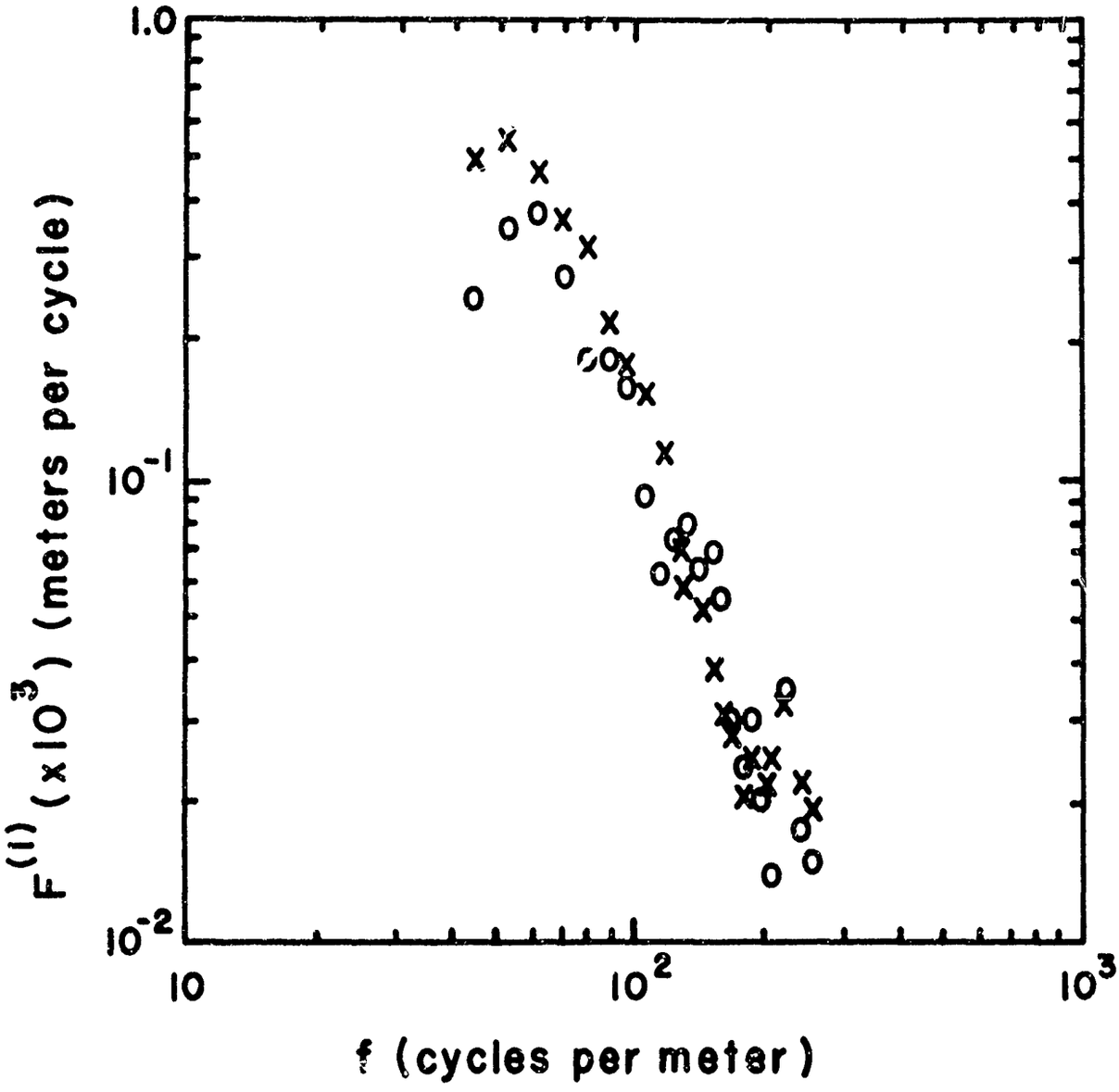

Figure 7. Vertical (O) and Horizontal (X) Scan Power Spectra for a 30 nsec Pulsed Ruby Laser

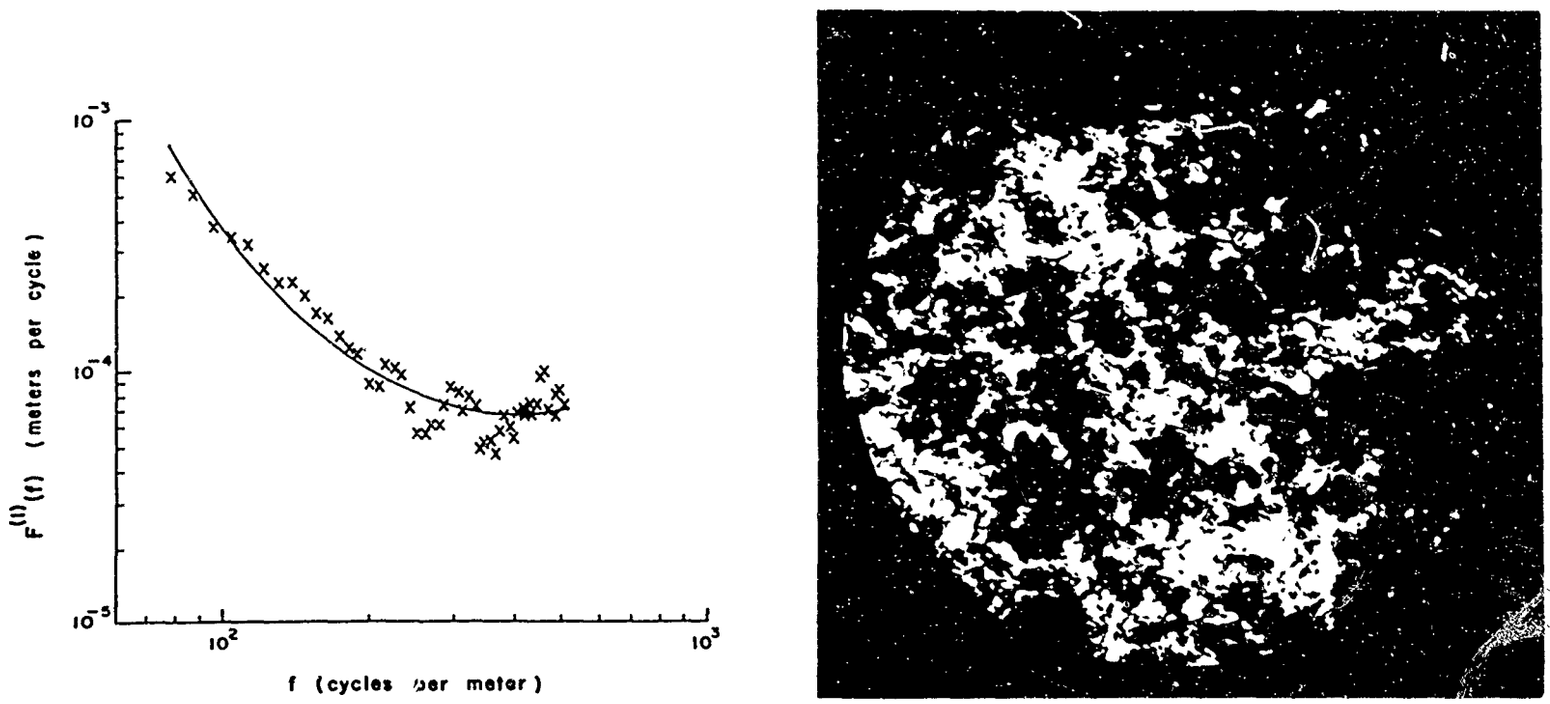

(a) (b)

Figure 8. Average Scan Power Spectra (a) and Associated Typical Photograph (b) for 1130h and 650-m Range

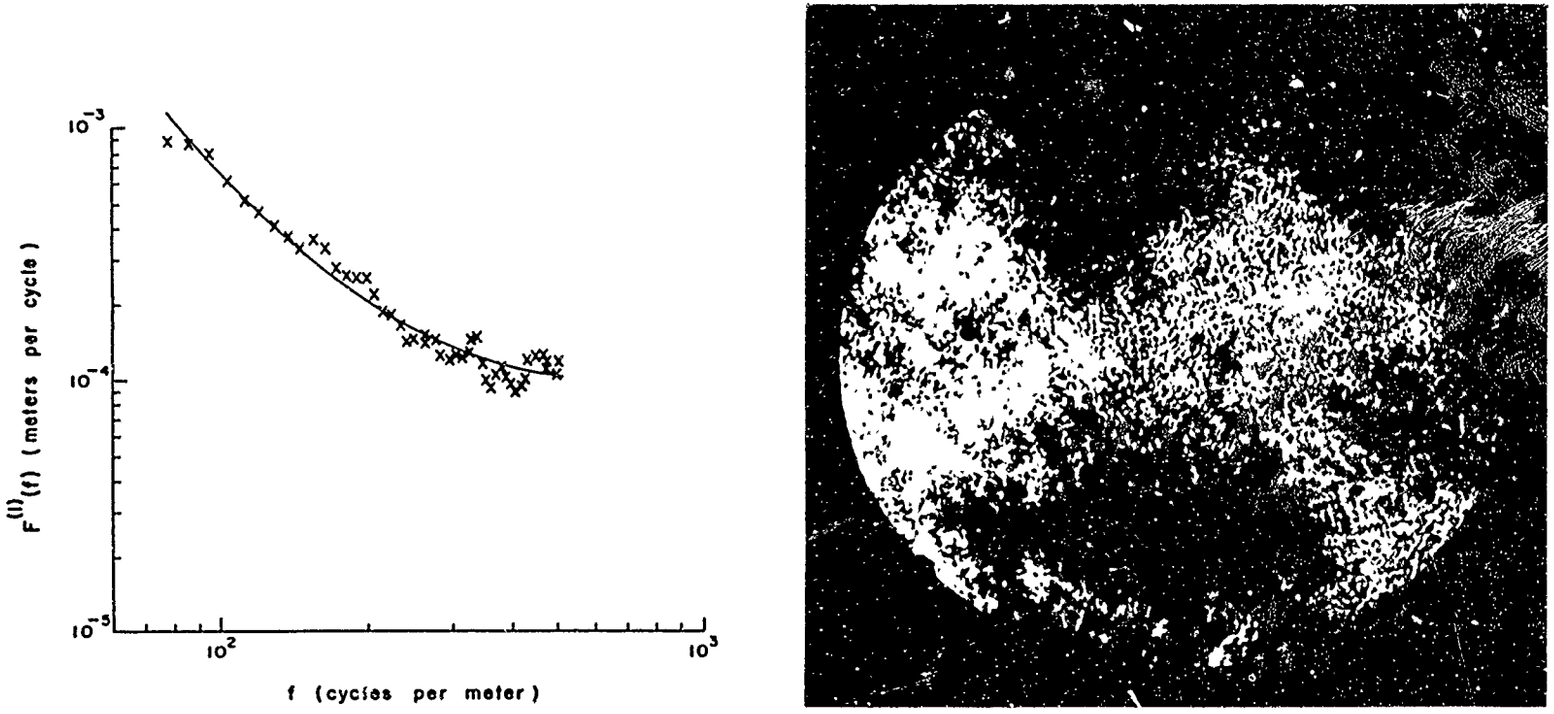

(a) (b)

Figure 9. Average Scan Power Spectra (a) and Associated Typical Photograph (b) for 1130h and 1300-m Range

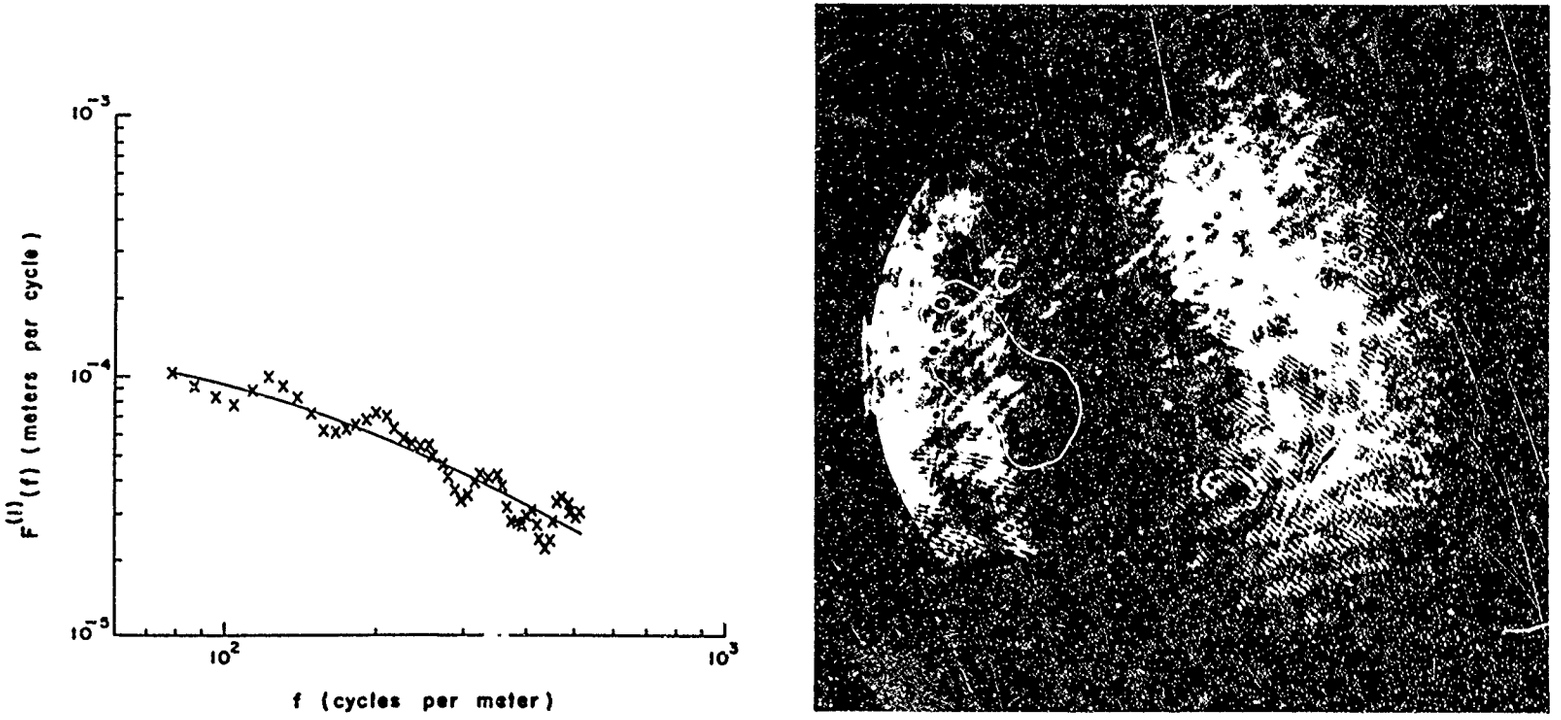

(a) (b)

Figure 10. Average Scan Power Spectra (a) and Associated Typical Photograph (b) for 1900h and 650-m Range

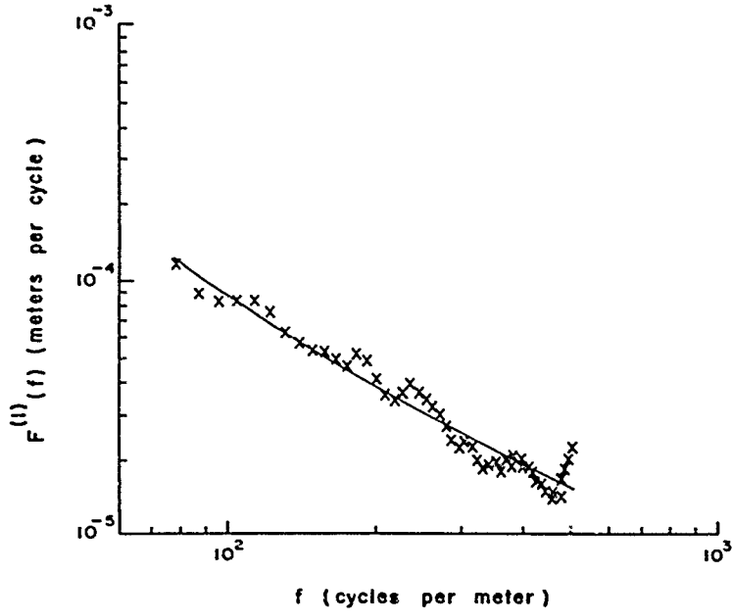

(a)

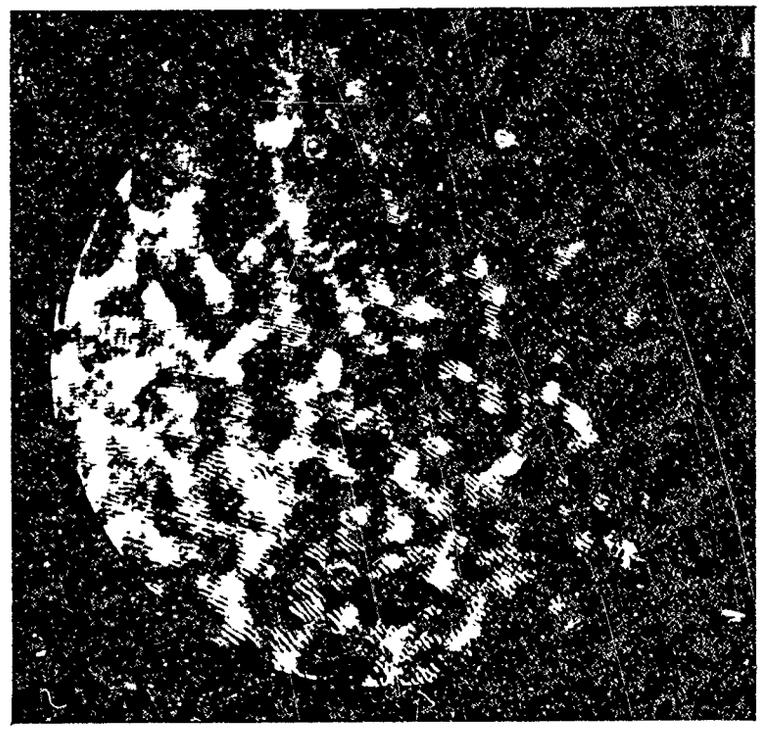

(b)

Figure 11. Average Scan Power Spectra (a) and Associated Typical Photograph (b) for 1900h and 1300-m Range

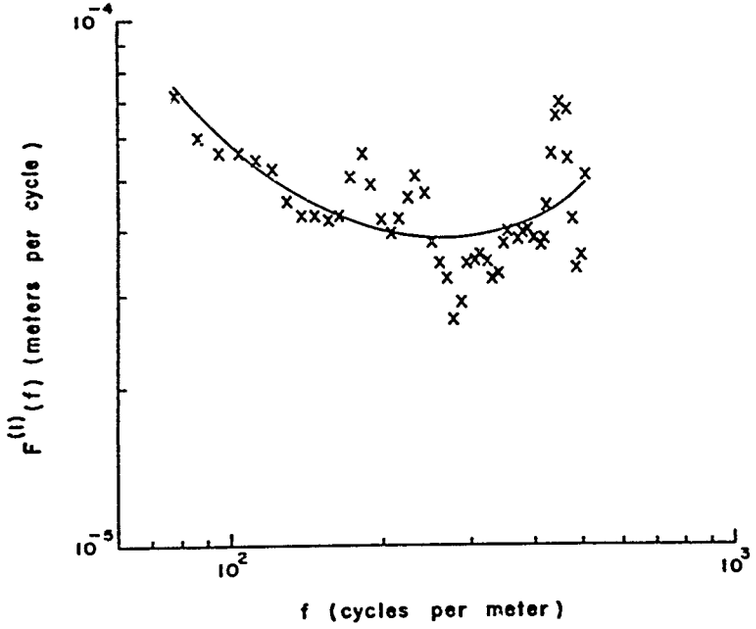

(a)

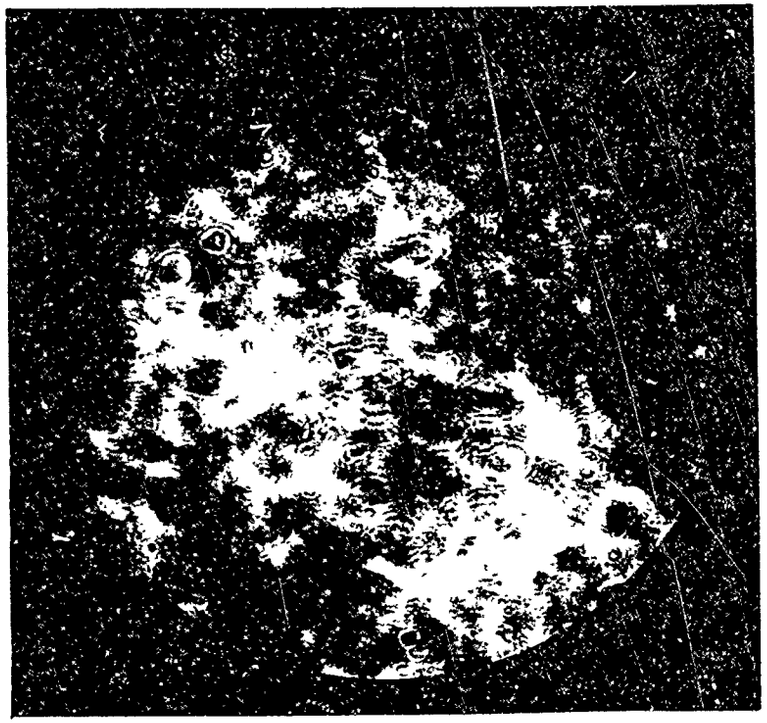

(b)

Figure 12. Average Scan Power Spectra (a) and Associated Typical Photograph (b) for 2200h and 650-m Range

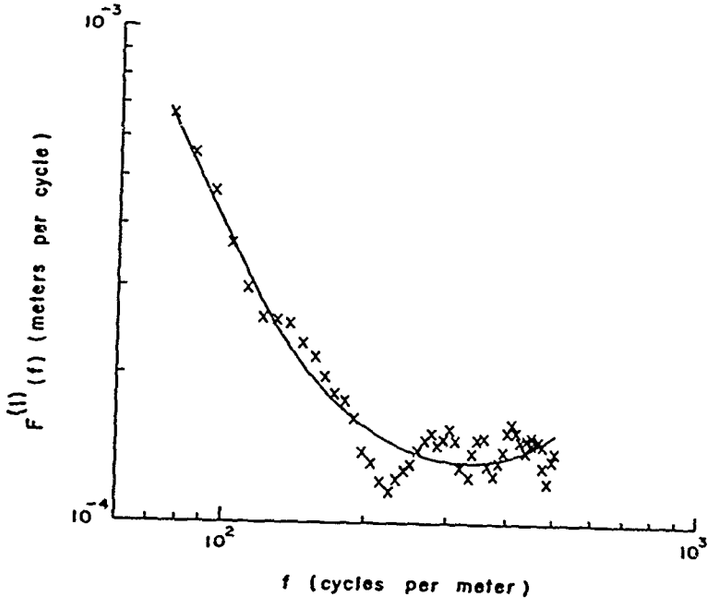

(a)

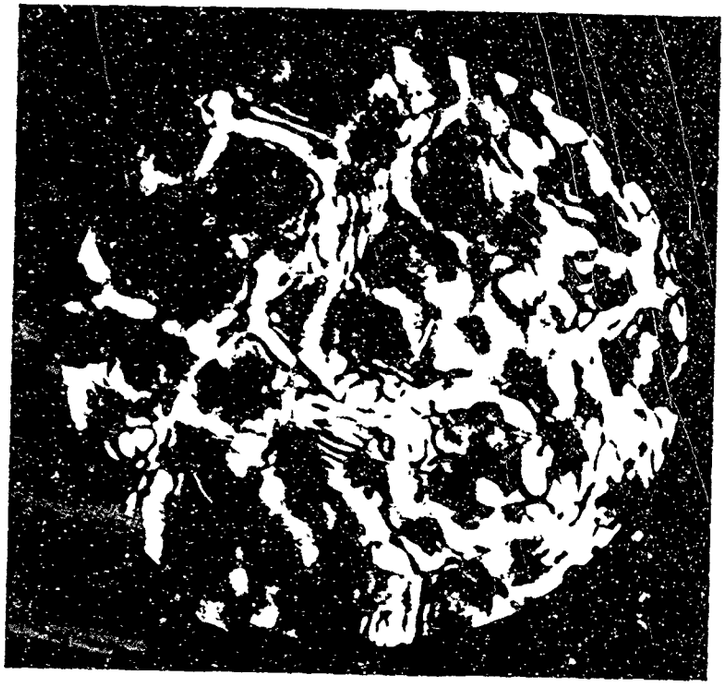

(b)

Figure 13. Average Scan Power Spectra (a) and Associated Typical Photograph (b) for 2200h and 1300-m Range

(1130 h). The scale of scintillation is reduced at the longer range as shown by the relative enhancement of the power at high frequencies. The large dark areas in Fig. 10 are due to a collimation problem. The digital filter applied to the data rejected the low frequencies associated with this effect, and thus the low-frequency data do not appear in the result. In these and all other spectra, the high-frequency tail is shown to curve up; such an effect is due to optical, film, and processing noise. The next set of spectra, Figs. 10 and 11, show beam photographs at nearly neutral conditions. Clearly, the power has dropped in the scintillation spectra at both ranges, and sufficient coherence remains in the received beam to produce coherence noise from various receiver elements. The difference of scintillation power at the two ranges appears the reverse of the photographs taken during lapse conditions. This fact and the observation that the peak power at 650 m is quite small suggest that during these conditions 650 m was still less than the transition distance between geometrical and Fresnel optical ranges. Accepting this conjecture, it might be concluded that the inner scale of turbulence was in the range of $2.1 < l_o < 5.8$ cm.

During inversion conditions, the relations of the two spectra, Figs. 12 and 13, are similar to those of the first pair taken under lapse conditions. Unfortunately, the large cells in Fig. 13 are below the cutoff in the power spectra and are not included.

C. Saturation of Statistics

Figure 3 gives the measured standard error of the log-irradiance versus the PST value plotted on the abscissa. The horizontal bars

represent the spread in C_n measurements made by various techniques as explained above, while the vertical bars give the spread in data points. The data lie above the deWolf curve (PMST) but cross it for large values of the abscissa. This decay of the measured standard error is considered real and experimentally reproducible. Such behavior is not predicted by the deWolf theory, but may be due to finite beam effects.

D. Optical Filter Function

As discussed in the body of this paper, the optical filter function is derivable from the data. The results are shown in Figs. 1 and 2. The curves marked PST and BST are plots of Eqs. (3) and (5) where parameters b and b_1 were fitted to our experiment. The dashed lines represent measured optical filter functions in the frequency range from 87 to 200 c/m for various runs. Data for which scintillation was comparable to system noise were eliminated. The direction of the dashed lines is considered significant in distinguishing between the PST and the BST treatments. The frequency range was chosen so that the data represent the inertial subrange of turbulence under most experimental conditions.

CONCLUSIONS

The photographic method of scintillation analysis represents several distinct advantages over the prevailing temporal sampling techniques. As discussed earlier, if a proper exposure time is chosen to freeze the smallest wavelengths, the data are sensibly independent

of the normal wind speed. Therefore, the uncertainty in the measurement of an average normal wind speed is eliminated. The "frozen-in" hypothesis need not be assumed. Finally, the statistical isotropy of the beam cross section can be investigated readily. Our experiment shows that within the frequency range examined the refractive-index fluctuations are essentially isotropic even at a mean height of 1½ m above the ground. Clearly, as lower spatial frequencies are resolved, this assertion must break down.

The decline of the saturation curve in Fig. 3 is considered real. Such behavior is not predicted by the PMST of deWolf and thus may represent a partial failure of the initial plane-wave assumption as a representation of a real beam.

Finally, the scan spectra, containing much more statistical information than the standard errors, may be used to force decisions between competing theories of light propagation by means of the optical filter calculation. Moreover, the optical filter function is relatively insensitive to the details of the index of refraction spectrum and consequently is a universal function dependent only on such parameters as optical wave number, path length, and beam divergence. Consequently, the optical filter calculations shown as dashed lines suggest better agreement with beam-wave theory than with the results of plane-wave predictions.

ACKNOWLEDGMENTS

The authors gratefully acknowledge the invaluable assistance of J. Evans in the measurements. In addition, thanks are expressed to J. Lanahan, J. Cope, M. Stansbury, T. Stanton, N. Wright, and R. Price.

REFERENCES

1. J. W. Strohbehn, *Proc. IEEE,* Vol. 56, 1968, p. 1301.

2. V. I. Tatarski, *Wave Propagation in a Turbulent Medium,* New York, McGraw-Hill Book Company, 1960.

3. A. Ishimaru, *Radio Sci.,* Vol. 4 (New Series), 1969, p. 295.

4. F. P. Carlson, *Bull. Opt. Soc. Am.,* WH19, March 1969.

5. V. I. Tatarski and A. I. Kon, Izv. Vuzov, *Radiofizika,* Vol. 8, 1965, p. 870. Here the authors consider only the perturbation in the phase structure function and, hence, the angle-of-arrival fluctuations. However, the beam profile is formulated in terms of a gaussian amplitude rather than a gaussian irradiance and is therefore not a solution for the TEM_{oo} mode beam.

6. M. E. Gracheva and A. S. Gurvich, Izv. Vuzov, *Radiofizika,* Vol. 8, 1965, p. 717.

7. P. H. Deitz and N. J. Wright, *J. Opt. Soc. Am.,* Vol. 59, 1969, p. 527.

8. V. I. Tatarski, *Soviet Phys. JETP,* Vol. 22, 1966, p. 1083.

9. V. I. Tatarski, *Soviet Phys. JETP,* Vol. 19, 1964, p. 946.

10. V. I. Tatarski and M. E. Gertsenshtein, *Soviet Phys. JETP,* Vol. 17, 1963, p. 458.

11. D. A. deWolf, *J. Opt. Soc. Am.,* Vol. 58, 1968, p. 461.

12. Ref. 2, p. 136.

13. J. M. Caborn, *British Forestry Comm. Bull.,* Vol. 29, 1950.

14. Ref. 2, p. 40.

15. Ref. 2, p. 79.

16. L. R. Tsvang, *Izvestia* ANSSSR, Geophys. Ser. 8, 1960, p. 1252.

17. Private correspondence through contract with Dr. D. J. Portman and co-workers, Department of Meteorology and Oceanography, University of Michigan, Ann Arbor.

18. P. H. Deitz, in *Modern Optics,* J. Fox, Ed., New York, Polytechnic Press, 1967, p. 766 ff.

19. Ref. 2, p. 215.

20. Phase measurements for these times are reported by R. Buser and G. Born, *J. Opt. Soc. Am.* (to be published).

21. Private communication with M. A. Martin.

22. R. B. Blackman and J. W. Tukey, *The Measurement of Power Spectra,* New York, Dover Publications, 1958.

APPENDIX A

Consider the following change of variables in Eq. (19):

$$x = \kappa^{-1}(\gamma^2 + \kappa^2)^{\frac{1}{2}} \tag{A-1}$$

Thus, Eq. (19) becomes

$$\phi^{(2)}(\kappa) = \frac{\phi^{(1)}(\kappa_o)}{\kappa\pi} \int_1^\infty \frac{dx}{(x^2 - 1)^{\frac{1}{2}}} \frac{d}{dx} \exp[A(\theta + \tilde{x}) + B(\theta + \tilde{x})^2] \tag{A-2}$$

where

$$\tilde{x} = \ln x \quad \text{and} \quad \theta = \ln(\kappa/\kappa_o). \tag{A-3}$$

The derivative with respect to x can be moved out of the integral since

$$\frac{d}{dx} \exp[A(\theta + \tilde{x}) + B(\theta + \tilde{x})^2] = x^{-1} \frac{d}{d\tilde{x}} \exp[A(\theta + \tilde{x}) + B(\theta + \tilde{x})^2] \tag{A-4}$$

and the expression is further simplified with the chain rule,

$$\frac{d}{d\theta} = \frac{d\kappa}{d\theta} \frac{d}{d\kappa} = \kappa \frac{d}{d\kappa} = \frac{d}{d\tilde{x}} \tag{A-5}$$

and by defining

$$\tilde{A} = A - 1.$$

Equation (A-2) then becomes

$$\phi^{(2)}(\kappa) = -\frac{\phi^{(1)}(\kappa_o)}{\pi} \frac{d}{d\kappa} \exp(A\theta + B\theta^2) \int_1^\infty \frac{dx}{(x^2 - 1)^{\frac{1}{2}}} \exp(\tilde{A}\tilde{x} + 2B\tilde{x}\theta + B\tilde{x}^2) \tag{A-6}$$

The exponent in the integrand can be expressed as an infinite series

$$\exp(\tilde{A}\tilde{x} + 2B\tilde{x}\theta + B\tilde{x}^2) = \exp[(\tilde{A} + 2B\theta)\tilde{x}] \sum_{k=0}^{\infty} \frac{(B\tilde{x}^2)^k}{k!}$$

$$= \sum_{k=0}^{\infty} \frac{1}{(4B)^k} \frac{\kappa^{2k}}{k!} \frac{d^{2k}}{d\kappa^{2k}} \exp[(\tilde{A} + 2B\theta)\tilde{x}] \tag{A-7}$$

Thus, Eq. (A-6) becomes

$$\phi^{(2)}(\kappa) = -\frac{\phi^{(1)}(\kappa_0)}{\pi}\frac{d}{d\kappa}\left[e^{a(\theta)}\sum_{k=0}^{\infty}\left(\frac{1}{4B}\right)^k\frac{\kappa^k}{k!}\frac{d^{2k}}{d\kappa^{2k}}G(\theta,\kappa)\right] \qquad (A\text{-}8)$$

where

$$G(\theta,\kappa) = \int_1^{\infty}\frac{dx}{(x^2-1)^{\frac{1}{2}}}x^{(\tilde{A}+2B\theta)} \qquad (A\text{-}9)$$

and

$$a(\theta) = A\theta + B\theta^2.$$

Consider the change of variable

$$x^2 = 1/r,$$

then Eq. (A-9) becomes

$$G(\theta,\kappa) = \frac{1}{2}\int_0^1 (1-r)^{-\frac{1}{2}}\, r^{-\frac{1}{2}(\tilde{A}+2B\theta)-1}\, dr.$$

But the integral is the definition of a beta function; thus

$$G(\theta,\kappa) = \frac{1}{2}\beta\left(\frac{1}{2}\,|\,\tilde{A}+2B\theta\,|\,;\frac{1}{2}\right). \qquad (A\text{-}10)$$

The beta function exists providing

$$(\tilde{A}+2B\theta) < -1.$$

Insertion of Eq. (A-10) into Eq. (A-8) gives Eq. (20) of the text.

It is also possible to treat Eq. (A-2) by an asymptotic method. Let

$$z = (|B|)^{\frac{1}{2}}\tilde{x},$$

then Eq. (A-9) becomes

$$G(\theta) = \frac{1}{(|B|)^{\frac{1}{2}}} \int_0^{\infty} \frac{\exp[M(\theta)\, z/((|B|)^{\frac{1}{2}} - z^2]}{\{1 - \exp[-2z/((|B|)^{\frac{1}{2}}]\}^{\frac{1}{2}}} dz \tag{A-11}$$

where

$$M(\theta) = \tilde{A} + 2B\theta. \tag{A-12}$$

Equation (A-11) can be expressed in terms of a power series in z^2. After expansion, Eq. (A-11) reduces to

$$G(\theta) = \frac{1}{2} \int_0^1 x^{-\frac{M(\theta)}{2} - 1} (1 - x)^{-\frac{1}{2}} dx \tag{A-13}$$

$$+ \frac{1}{2} \sum_{m=1}^{\infty} \frac{(-1)^m}{m!} \frac{|B|^m}{2^{2m}} \int_0^{\infty} \exp[2m \ln y - \frac{|M(\theta)|}{2} y - \frac{1}{2} \ln(1 - e^{-y})]dy.$$

The first term in Eq. (A-13) is a beta function and the remaining series can be evaluated by the saddle point technique. The integral is absolutely convergent though the sum may only be asymptotically convergent. The integrand is peaked at a root of

$$f'(y) = \frac{2m}{y} - \frac{|M(\theta)|}{2} - \frac{1}{2(1 - e^{-y})} = 0. \tag{A-14}$$

An approximate root of this equation is readily extracted,

$$y_o \simeq \frac{2(2m - \frac{1}{2})}{|M(\theta)|}, \tag{A-15}$$

providing y_o is sufficiently small that

$$1 - e^{-y} \sim y.$$

Conversely, if y_o is large, then

$$y_o \approx \frac{4m}{|M(\theta)| + 1} . \tag{A-16}$$

Both estimates reduce to the same value if $2m > \frac{1}{2}$ and $|M(\theta)| > 1$.

At the saddle point,

$$f(y) \approx (2m - \tfrac{1}{2}) \ln y_o - \frac{|M(\theta)|}{2} y_o . \tag{A-17}$$

Hence

$$\int_0^\infty dy\, e^{f(y)} \approx e^{f(y_o)} \int_0^\infty \exp\left[-\frac{1}{2} |f''(y_o)| (y - y_o)^2 dy\right]$$

$$\approx e^{f(y_o)} \left(\frac{\pi}{2|f''(y_o)|}\right)^{\frac{1}{2}} \left[1 + \operatorname{erf}\{(f''(y_o) y_o/2)^{\frac{1}{2}}\}\right] .$$

A saddle point exists provided $f''(y_o) < 0$. For the above case,

$$|f''(y_o)| = \frac{|M(\theta)|^2}{4(2m - \frac{1}{2})} . \tag{A-18}$$

Thus an approximation for $G(\theta)$, Eq. (A-13), may be written as

$$G(\theta) \approx \tfrac{1}{2}\beta(|M(\theta)|/2; \tfrac{1}{2})$$

$$+ \frac{1}{2} \sum_{h=1}^{w} \frac{|B|^n (-1)^n}{n!\sqrt{2}} \frac{\Gamma(2n + \frac{1}{2})}{|M(\theta)|^{2n+\frac{1}{2}}} \{1 + \operatorname{erf}[(m - \tfrac{1}{4})^{\frac{1}{2}}]\} \tag{A-19}$$

where the summation cutoff, w, represents the convergence "radius" for the series. The approximate value of w is

$$w = \frac{4\, M(\theta)^2}{|B|} \tag{A-20}$$

The expression derived for $G(\theta)$, Eq. (A-19), may be inserted into Eq. (A-8) to give an expression for $\Phi^{(2)}(\kappa)$ suitable for computer evaluation:

$$\phi^{(2)}(\kappa) = -\frac{\phi^{(1)}(\kappa_o)}{2\pi\kappa_o}\left(\frac{\kappa}{\kappa_o}\right)^{[A - 1 + B\ \ln(\kappa/\kappa_o)]} \qquad [A + 2B\ \ln(\kappa/\kappa_o)]Q \qquad \text{(A-21)}$$

where

$$Q = \beta(|M(\theta)|/2;\ \tfrac{1}{2})\left\{1 + \frac{BM(\theta)}{|M(\theta)|[1 + M(\theta)]}\, q\left(\frac{|M(\theta)|}{2}\right)\right\}$$

$$+ \frac{1}{\sqrt{2}} \sum_{n=1}^{w} \left\{ C_n + \frac{2B}{|M(\theta)|}\left(\frac{\theta}{1 + M(\theta)}\right) D_n \right\} \qquad \text{(A-22)}$$

and

$$C_n = |B|^n(-1)^n \frac{\Gamma(2n + \tfrac{1}{2})}{\Gamma(n+1)\ |M(\theta)|^{\frac{1}{2}}}\{1 + \text{erf}\ [(n - \tfrac{1}{4})^{\frac{1}{2}}]\}, \qquad \text{(A-23)}$$

$$D_n = |B|^n(-1)^{n+1} \frac{\Gamma(2n + 3/2)}{\Gamma(n+1)\ |M(\theta)|^{2n+3/2}}\{1 + \text{erf}\ [(n - \tfrac{1}{4})^{\frac{1}{2}}]\}, \qquad \text{(A-24)}$$

$$q\left(\frac{|M(\theta)|}{2}\right) = \psi\left(\frac{|M(\theta)|}{2}\right) - \psi\{\tfrac{1}{2}[1 + |M(\theta)|]\}. \qquad \text{(A-25)}$$

The ψ functions are the tabulated derivatives of the log gamma functions. In the event that B = 0,

$$Q = \beta(|M(\theta)|/2;\ \tfrac{1}{2}) \qquad \text{(A-26)}$$

and Eq. (21) becomes

$$\phi^{(2)}(\kappa) = -\frac{\phi^{(1)}(\kappa_o)}{2\pi\kappa_o}\left(\frac{\kappa}{\kappa_o}\right)^{A-1} A\,\beta(|A - 1|/2;\ \tfrac{1}{2}). \qquad \text{(A-27)}$$

But this is just the expression for a simple power law fit of a one-dimensional scan spectrum with slope A.

APPENDIX B

It is useful to estimate the effect wind transport of turbulence has on the high spatial frequency components of the scintillation spectra. A convenient way of expressing such a calculation is by means of an exposure transfer function. The relation between the structure function, D_f, of a quantity $f(x,y,z)^2$ and its associated power spectrum in the constant z plane is

$$D_f(x-x',y-y') = 2\iint_{-\infty}^{\infty} d\kappa_1 d\kappa_2 \{1 - \cos[\kappa_1(x-x') + \kappa_2(y-y')]\}F_f(\kappa_1,\kappa_2,0). \tag{B-1}$$

We will suppose that a wind, with velocity v_x, blows normally across the beam path and transports turbulence "frozen in" the wind stream across the beam path. This means, essentially, that the current values of x,x' (for a constant structure function) are related to the previous ones by

$$x = x'' - v_x t; \quad x' = x''' - v_x t'. \tag{B-2}$$

Since we are assuming stationary processes, it follows that D_f can only depend upon the difference in the times. Thus,

$$D_f[x-x' - v_x(t-t'),y-y'] \tag{B-3}$$

$$= 2\iint_{-\infty}^{\infty} d\kappa_1 d\kappa_2 \{1 - \cos[\kappa_1(x''-x''') + \kappa_2(y-y') - v_x\kappa_1(t-t')]\}F_f(\kappa_1,\kappa_2,0).$$

Let the function f represent the instantaneous log-amplitude, and let the exposure averaged function be defined as

$$D_f(x''-x''',y-y')_{av} = \frac{1}{\tau^2}\int\int_0^\tau dtdt' D_f[x''-x''' - v(t-t'),y-y'] \qquad (B-4)$$

where τ is the exposure time. A reasonable assumption is that the exposure time average is interchangeable with the integration in Eq. (B-3). Consequently, we find

$$D_f(x''-x''',y-y')_{av} \qquad (B-5)$$

$$= 2\int\int_{-\infty}^{\infty} d\kappa_1 d\kappa_2 \{1 - \frac{1}{\tau^2}\int\int_0^\tau dtdt' \cos[\kappa_1(x''-x''') + \kappa_2(y-y') - v_x\kappa_1(t-t')]\}$$

$$\times F_f(\kappa_1,\kappa_2,0).$$

The integration over time is best accomplished by changing variables to the average and difference in time. Then let the spectrum of $D_x(x''-x''',y-y')_{av}$ be defined as

$$D_f(x''-x''',y-y')_{av}$$

$$= 2\int\int_{-\infty}^{\infty} \{1 - \cos[\tilde{\kappa}_1(x''-x''') + \tilde{\kappa}_2(y-y')]\}F_f{}^{av}(\tilde{\kappa}_1,\tilde{\kappa}_2,0)\, d\tilde{\kappa}_1 d\tilde{\kappa}_2 \qquad (B-6)$$

A comparison of Eq. (B-6) and the integrated form of Eq. (B-5) gives the relation between the spectra

$$F_f{}^{av}(\underline{\kappa},0) = \frac{2}{(\underline{\kappa}\cdot\underline{v})^2\tau^2}\,[1 - \cos(\underline{\kappa}\cdot\underline{v}\tau)]\; F_f(\underline{\kappa},0). \qquad (B-7)$$

The exposure transfer function,

$$T(\underline{\kappa},0) = \frac{2}{(\underline{\kappa}\cdot\underline{v})^2\tau^2}\,[1 - \cos(\underline{\kappa}\cdot\underline{v}\tau)], \qquad (B-8)$$

is then readily identified. The spatial frequency for which the transfer function has its first zero is

$$f = 500/V \text{ cycles/m} \qquad \text{(B-9)}$$

for the experimental exposure of 2 msec. A fit to the data of Fig. 6 at a spatial frequency of 250 cycles/m would require a computed normal wind speed of approximately 2 m/sec, compared with the measured wind speed of 2.16 m/sec.

Unclassified

Security Classification

DOCUMENT CONTROL DATA - R & D

Security classification of title, body of abstract and indexing annotation must be entered when the overall report is classified)

1 ORIGINATING ACTIVITY (Corporate author)	2a. REPORT SECURITY CLASSIFICATION
U. S. Army Aberdeen Research and Development Center Ballistic Research Laboratories Aberdeen Proving Ground, Maryland 21005	Unclassified 2b. GROUP

3 REPORT TITLE

COHERENT LIGHT PROPAGATION THROUGH A TURBULENT ATMOSPHERE: MEASUREMENTS OF THE OPTICAL FILTER FUNCTION

4 DESCRIPTIVE NOTES (Type of report and inclusive dates)

5 AUTHOR(S) (First name, middle initial, last name)

Peter M. Livingston, Paul H. Deitz, and Ernest C. Alcaraz

6 REPORT DATE	7a. TOTAL NO. OF PAGES	7b. NO. OF REFS
October 1969	61	22

8a. CONTRACT OR GRANT NO.	9a. ORIGINATOR'S REPORT NUMBER(S)
b. PROJECT NO. RDTE 1T061102A31C	Memorandum Report No. 2018
c.	9b. OTHER REPORT NO(S) (Any other numbers that may be assigned this report)
d.	

10 DISTRIBUTION STATEMENT

This document has been approved for public release and sale; its distribution is unlimited.

11 SUPPLEMENTARY NOTES	12. SPONSORING MILITARY ACTIVITY
	U. S. Army Materiel Command Washington, D. C. 20315

13 ABSTRACT

Two He-Ne lasers operating at 6328 Å have been utilized to make simultaneous measurements of the effects of scintillation over homogeneous optical paths of 650 and 1300 m to study the transfer of coherent radiation through a turbulent medium. At the path terminus, multiple sampling of each laser beam was effected using a photo-optical technique which records a 61-cm cross section of an optical beam. Concurrent with the optical data, wind-speed and direction recordings were made at multiple points along the optical path in order to estimate the homogeneity of meteorological conditions. Near the path terminus, measurements of wind shear and temperature lapse were taken. In addition, high-speed thermometry techniques were utilized to compute one-dimensional temperature spectra as well as the thermal structure coefficient C_T. Data were gathered during temperature-lapse, neutral, and inversion conditions. Log-irradiance scans derived from the optical data were used to compute log-irradiance power spectra, variance, and other statistical quantities. Using these optical and meteorological data, optical filter functions were then calculated for spatial frequencies above 87 c/m and are used to compare with current theories. The saturation of the log-irradiance data is again observed, and the isotropy of the irradiance fluctuations is examined.

DD FORM 1 NOV 1473 REPLACES DD FORM 1473, 1 JAN 64, WHICH IS OBSOLETE FOR ARMY USE.

Unclassified

Security Classification

14 KEY WORDS	LINK A		LINK B		LINK C	
	ROLE	WT	ROLE	WT	ROLE	WT
Scintillation						
Atmospheric turbulence						
Atmospheric optics						
Inhomogeneous media						
Propagation						